A membrane interferometer

Prasad V. Ganesan and Steven G. Boxer[1]

Department of Chemistry, Stanford University, Stanford, CA 94305-5080

Contributed by Steven G. Boxer, February 16, 2009 (sent for review December 10, 2008)

Freestanding phospholipid bilayers have been assembled spanning shallow, micrometer-sized wells etched into a Si wafer substrate so that the bilayers are near (within hundreds of nanometers) but not in contact with the wafer surface. The proximity of the bilayers to the highly reflective Si/SiO_2 interface allows them to be probed by using fluorescence-interference techniques. These interferometry measurements show that the bilayers are curved and that the curvature can be varied by changes in osmotic pressure. Furthermore, the ionophore gramicidin can be incorporated into the bilayers, making them selectively permeable to monovalent cations. This freestanding architecture may overcome surface-interaction problems that occur when cell membrane proteins are introduced into solid supported bilayers, while also allowing for high-precision measurements of changes in fluorophore position by interferometry.

bilayer lipid membrane | black lipid membrane | fluorescence interference contrast

Bilayer or "black" lipid membranes (BLMs) are a widely used model system for the study of cell-membrane proteins (1). BLMs are prepared on an aperture, usually hundreds of micrometers in diameter, made in a hydrophobic substrate material. Advances in BLM platform architectures, particularly chip-based architectures, have been directed toward a range of different membrane geometries (2–5), improved reproducibility (6, 7) and stability (8, 9), and applying imaging techniques such as fluorescence microscopy (10–14). In parallel, efforts are ongoing to increase the utility of solid supported lipid bilayers (15, 16) for examining cell membrane proteins, including tethering (17), cushioning (18), and loosely associated second-story bilayers (19–21).

We are particularly interested in using fluorescence to study membrane protein conformational dynamics in a native environment, but measuring small changes requires the determination of fluorophore position with a precision better than the optical diffraction limit. The interference pattern above a mirror can be used to determine the absolute distance of fluorescent objects from the mirror with high precision (22). The mirror reflects excitation light, and the reflected light interferes with the incident light so that the intensity of excitation (and similarly, the intensity of emitted light) varies with distance from the mirror. To that end, we have developed a platform consisting of a freestanding lipid bilayer, analogous to a BLM, suspended above a reflective Si mirror (Fig. 1*A*).

In fluorescence interference contrast (FLIC) microscopy (22–25), this interferometry concept was adapted to determine distances of interest and distribution of fluorophores in SiO_2-supported lipid bilayers and associated objects, often with subnanometer precision. The bilayers are assembled on a SiO_2/Si wafer (because Si reflects visible light), with SiO_2 layers of varying thickness (sometimes called a FLIC-chip), to step the fluorophore through the interference pattern and generate multiple fluorescence intensity data points required for the absolute determination of the distance between the fluorophore and the SiO_2 substrate. This canonical FLIC method is not applicable for absolute distance determinations in freestanding bilayers because the bilayer is not associated directly with the substrate surface and so its distance from the mirror is not under lithographic control (although in some cases variations in surface-fluorophore distance can be inferred from fluorescence intensity variations) (20, 21). Two alternative strategies for determining distance parameters are applied here: variation of the incidence angle of excitation (variable incidence angle FLIC, or VIA-FLIC) (26) and the use of the 2 different bilayer-associated fluorophores in the system, 1,1′-dioctadecyl-3,3,3′,3′-tetramethyl-indo-carbocyanine (DiI) and Cy5, each with different wavelengths of excitation and emission (2-color or 2C-FLIC). As described in detail in the following (see *Results*), these methods were used to measure the water-layer thickness under the bilayer (d_{H_2O} in Fig. 1*A*, hundreds of nanometers) and show that the bilayers have a slight downward concavity.

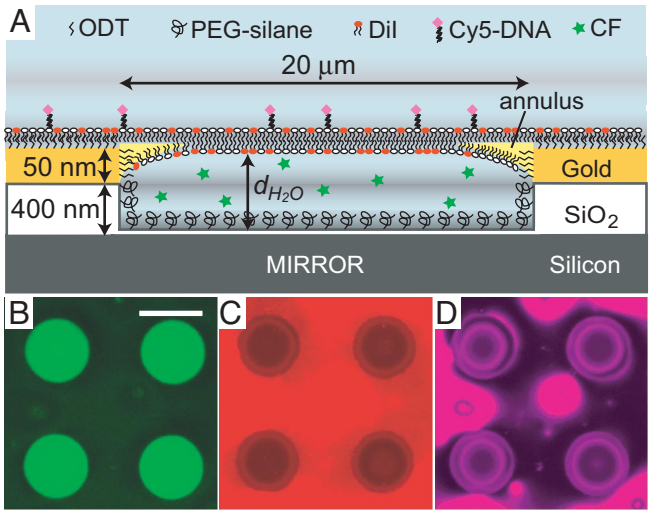

Fig. 1. A membrane interferometer. (*A*) Schematic diagram of a freestanding bilayer positioned within a few hundred nanometers of a Si mirror (the drawing is not to scale). (*B–D*) Fluorescence from CF (*B*), DiI (*C*), and Cy5-DNA (*D*) from 4 wells with freestanding bilayers. Note bright and dark rings for DiI and Cy5-DNA fluorescence over wells. (Scale bar: 20 μm.)

Results

Substrate Design. A substrate was designed to allow assembly of a lipid bilayer within a few hundred nanometers of a flat mirror so it can be probed by FLIC (Fig. 1*A*). Shallow wells were patterned on a Si wafer. The top of the wells needed to have a hydrophobic layer in order to imitate the surface properties of BLM apertures; the bottom surface and side walls needed to be functionalized to hinder lipid adhesion and yet be highly hydrophilic so the wells could be readily wetted; and the flat Si/SiO_2 interface would act as a mirror for interferometry at visible

Author contributions: P.V.G. and S.G.B. designed research; P.V.G. performed research; P.V.G. contributed new reagents/analytic tools; P.V.G. and S.G.B. analyzed data; and P.V.G. and S.G.B. wrote the paper.

The authors declare no conflict of interest.

[1]To whom correspondence should be addressed at: 380 Roth Way, Stanford, CA 94305-5080. E-mail: sboxer@stanford.edu.

This article contains supporting information online at www.pnas.org/cgi/content/full/0901770106/DCSupplemental.

wavelengths. Our most successful design used the orthogonal surface chemistries of exposed Au and SiO_2 thin films (see *Methods*, *SI Text*, and Fig. S1). First, exposed Au was functionalized with a self-assembled monolayer of octadecanethiol giving a hydrophobic surface. Next, exposed SiO_2 in the wells was functionalized with 2-[methoxy(polyethyleneoxy)propyl-]trimethoxysilane (PEG-silane, Gelest) to prevent nonspecific adsorption of lipid on the well surfaces (27).

Bilayer Formation. Spanning lipid bilayers were formed by the thinning of a 3-layer water/oil/water system (see *SI Text* and Fig. S2 for detailed description). A surface-functionalized chip as described above was immersed in a buffer containing the aqueous dye carboxyfluorescein (CF), then pure decane was spread with a pipette tip on the surface to form a macroscopically observable droplet, trapping CF in the wells. After CF had been washed out of the bulk upper water layer, phospholipids were added as small unilamellar vesicles doped with DiI. The vesicles were also decorated with a dye-labeled, DNA-lipid conjugate, where a 24-mer DNA oligonucleotide was anchored to the lipid at the 5′ end and Cy5 was added at the 3′ end (Cy5-DNA) (28). The partitioning of phospholipids into the decane led to a reduced contact angle of decane on the Au-self-assembled monolayer in water and rapid thinning to a decane film.

The decane film continued to thin until freestanding bilayers corresponding to Fig. 1*A* formed spontaneously, or alternatively, bilayers were formed by mechanically spreading the decane film with a small air bubble. The CF trapped in the wells by the decane layer could be clearly visualized, verifying that a discrete, aqueous compartment was trapped beneath the forming bilayer (Fig. 1*B*). Distinct bright and dark rings were observed over the wells for both DiI and Cy5-DNA fluorescence (Fig. 1 *C* and *D*); these occur because of interference of excitation light and emitted fluorescence with light reflected from the Si mirror at the bottom of the wells. The observed intensity variation indicates that bilayers, once formed, are slightly curved and this curvature is quantified below (see *Interferometry*). On the timescale of video imaging (≈100 ms per frame), the rings did not move, indicating that the bilayer curvature and position did not change appreciably. The edge of the receding decane film could be observed in fluorescence microscopy images of DiI and Cy5-DNA (Fig. S3). Bilayers could be distinguished from decane films by their location in areas where the decane film had visibly receded. Also, where films were present, the Cy5-DNA fluorescence was uniform rather than having interference rings.

Because the current design does not incorporate electrodes, the classical test for bilayer formation in freestanding BLMs, specific capacitance (29) could not be used. As an alternative test, the heavy-atom quencher Co^{2+} (25) was introduced into the upper aqueous layer and was shown to reversibly quench 100% of Cy5-DNA fluorescence and 50% of DiI fluorescence (*SI Text* and Fig. S4*A*). The result is consistent with Cy5-DNA being confined to the upper decane/water interface because of its high negative charge and consequent insolubility in bulk decane, whereas DiI is fully soluble in decane and equally partitioned between the upper and lower leaflet. Also, fluorescence recovery after photobleaching (FRAP) showed lateral fluidity, as would be expected for a lipid bilayer, and that the BLMs were continuous with the surrounding lipid on the gold surface (Fig. S4*B*).

Incorporation of Gramicidin. To show that the features observed over the wells were lipid bilayers, an additonal test was performed. This test incorporated the ionophore gramicidin and demonstrated its functionality. Gramicidin is a small peptide that inserts as monomers that span a single leaflet of the bilayer; passive and selective transport of monovalent cations occurs via transient dimers formed by monomers in the 2-bilayer leaflets (Fig. 2*A*) (30, 31). Gramicidin functionality was tested by measuring the pH (and hence H^+ transport) in the trapped well solution by using CF fluorescence intensity as a readout. The CF trapped in the lower water layer has a pK_a of 6.4, and the low pH form is much less fluorescent.

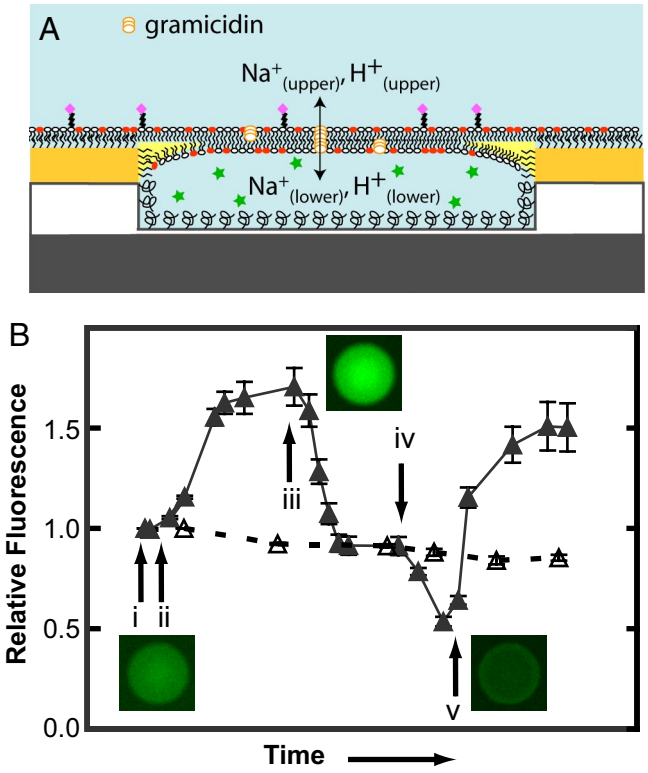

Fig. 2. Gramicidin incorporation mediates pH changes for aqueous solution trapped in wells. (*A*) Schematic diagram showing pore formation by a gramicidin dimer (orange ovals) and the species participating in the monovalent cation exchange equilibrium. (*B*) Effect of pH and NaCl concentration perturbations on CF fluorescence intensity in wells where the bilayer either contains gramicidin (solid triangles, $n = 10$) or does not (open triangles, $n = 15$): (i) initially, $pH_{(lower)} = 6.0$; (ii) $pH_{(upper)}$ is gradually increased to 7.2; (iii) $pH_{(upper)}$ is reduced to 6.0; (iv) $Na^+_{(upper)}$ is replaced with Mg^{2+} at equivalent osmotic strength and $pH_{(upper)}$ is increased to 7.2 simultaneously; and (v) $Na^+_{(upper)}$ is increased and $pH_{(upper)}$ maintained at 7.2, replacing Mg^{2+}. (*Insets*) CF fluorescence images of a well at identical contrast at stages i, iii, and v.

Small amounts of gramicidin were added to the lipid mixture used to make bilayers in 0.50 M NaCl at pH 6.1 so that CF fluorescence was initially dim (Fig. 2*B*, stage i). The presence of gramicidin would be expected to establish an exchange equilibrium between the trapped aqueous volume and the bulk upper water:

$$Na^+_{(upper)} + H^+_{(lower)} \rightleftharpoons Na^+_{(lower)} + H^+_{(upper)} \quad K = 1. \qquad [1]$$

From this equilibrium, $a_{Na^+(lower)}/a_{Na^+(upper)} = a_{H^+(lower)}/a_{H^+(upper)}$, with a defined as the activities of the respective solutes. In the experiment, $[Na^+] = 0.5\ M \gg [H^+] \approx 10^{-7}\ M$. Also, the upper water layer is much larger in volume than the lower layer, meaning that $[H^+_{(lower)}]$, and hence $a_{H^+(lower)}$, is the most sensitive component in the equilibrium expression, and the other components can be assumed to be constant as the system equilibrates. Conveniently, $a_{H^+(lower)}$ is directly related to the intensity of the CF fluorescence signal.

The bulk pH, $pH_{(upper)}$, was gradually changed by 5×1 mL washes of the upper water layer with 0.50 M NaCl in pH 7.1 buffer (Fig. 2*B*, stage ii). After each wash, CF fluorescence images of 10 wells with bilayers were collected, showing an

increase in intensity of ≈60%. This increase indicated that $pH_{(lower)}$ increased to reestablish the equilibrium induced by the presence of gramicidin. Two additional fluorescence images were taken to establish that this equilibrium had been reached. Then the sample was washed with 5 × 1 mL 0.50 M NaCl at pH 6.1 (Fig. 2*B*, stage iii) and CF fluorescence images collected as in stage ii. The CF fluorescence returned to its original value, as expected, on returning $pH_{(upper)}$ to 6.1.

Next, the sample was washed with 2 × 3 mL of 0.33 M $MgCl_2$ at pH 7.1 (Fig. 2*B*, stage iv). This perturbation represented 3 changes: $[Na^+_{(upper)}]$ decreased to ≈0, $[H^+_{(upper)}]$ decreased by ≈10×, and $[Mg^{2+}_{(upper)}]$ was introduced. If the bilayer were permeable to all 3 cations, then $pH_{(lower)}$ would be expected to increase, leading to an increase in CF fluorescence intensity. Instead, the CF signal decreased, indicating $pH_{(lower)} < 6.1$. This result is consistent with Eq. **1**, i.e., the bilayers' permeability is conferred by gramicidin and applies only to monovalent cations. According to this equation, $a_{Na^+(lower)}/a_{Na^+(upper)} \rightarrow \infty$ as a result of the perturbation in Fig. 2*B*, stage iv, so $a_{H^+(lower)}$ would indeed increase, even though $a_{H^+(upper)}$ decreased. Further confirming this effect, the sample was washed with 4 × 1 mL 0.50 M NaCl at pH 7.1 (stage v) to remove the Na^+ concentration gradient, and $pH_{(lower)}$ increased to match $pH_{(upper)}$. Additional experiments showed that gramicidin-containing decane films did not exhibit pH dependent CF fluorescence intensity variation (see Fig. S5).

Interferometry. In VIA-FLIC, varying the incidence angle of excitation light, θ_{inc}, on the Si mirror surface modulates the interference pattern of the excitation, resulting in different patterns of observed fluorescence intensity (Fig. 3*A*). Because the wells were approximately circularly symmetric, fluorescence intensity was analyzed as a function of distance from the center of the well, *r*. Fig. 3*B* shows fluorescence intensity vs. *r* for DiI over a single well for 10 narrow ranges of θ_{inc} values between 10° and 29°. These data were initially fit by using a VIA-FLIC model in which data for each value of *r* were fit separately (the "discrete model"). The parameter of interest in each fit was the water layer thickness, d_{H_2O} (Fig. 1*A*). The set of d_{H_2O} values obtained with the discrete model is plotted as black points in Fig. 3*C*. Because these values appeared to follow a circular arc, the data were also fit by using a model with 2 geometric variables, the height at the center, d_0, and the radius of curvature, R_c (the "spherical cap" model, see *Materials and Methods*). This fit is also plotted in Fig. 3*C*, with d_0 = 728 nm and R_c = 168 μm.

Fluorescence data for 2C-FLIC analysis were obtained by using normal epifluorescence excitation. Fluorescence intensity as a function of *r*, for the same well as in Fig. 3, is plotted for DiI and Cy5-DNA in Fig. 4. These data were fit with a spherical cap model, with best-fit geometric parameters d_0 = 734 nm and R_c = 167 μm, closely matching results obtained from VIA-FLIC.

Error estimates from the Matlab optimization for d_0 and R_c were very small. To better estimate the experimental error, VIA-FLIC and 2C-FLIC parameter determinations were performed for 10 wells. The VIA-FLIC spherical cap parameters for these 10 wells, with error bars marking the difference between the fits obtained from the 2 models, are plotted in Fig. 5, as d_0 vs. $1/R_c$. VIA-FLIC results are also shown for 4 additional wells not fit by FLIC. If spherical cap bilayers have a fixed point of contact (r_{edge}, d_{edge}) with the underlying hard substrate, the following relationship between d_0 and R_c in terms of (r_{edge}, d_{edge}) can be derived (*SI Text* and Fig. S6):

$$d_0 = (r_{edge}^2/2)(1/R_c) + d_{edge}. \quad [2]$$

Linear regression analysis of the points in Fig. 5 yields values of r_{edge} and d_{edge} of 9.4 ± 0.2 μm and 440 ± 10 nm, respectively. The expected radius and well depths for these substrates were 10 μm and ≈450 nm (400 nm of SiO_2 and 50 nm of Au with a 5-nm Ti adhesion layer), respectively, thus the values obtained from interferometry match the expected values based on the fabrication process.

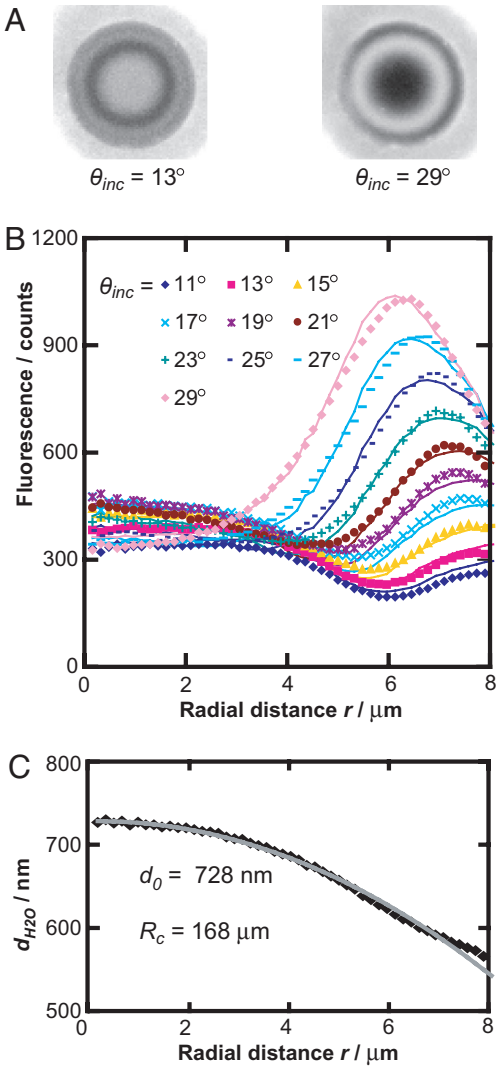

Fig. 3. VIA-FLIC of bilayer curvature. (*A*) DiI fluorescence images of a well with excitation angles (θ_{inc}) of 13° and 29°. (*B*) DiI fluorescence intensity vs. *r* where *r* is the distance from the middle of the well, for 10 θ_{inc} values (labeled), with corresponding fits from the 2 parameter, spherical cap model (see *Materials and Methods*). (*C*) Values of d_{H_2O} from a discrete VIA-FLIC model fit (black diamonds) and the spherical cap fit (gray line) to the data in *B*. Values for d_0 and R_c are marked (see Fig. S6 for geometric analysis).

Effect of Salt Concentration. Bilayer position and curvature could be affected by changing osmotic pressure, as shown by changes in the fluorescence pattern over the wells (Fig. 6 shows one example). This change was quantified with 2C-FLIC for 6 wells at $[Na^+_{(upper)}]$ of 0.50 M and 0.53 M. The spherical cap parameters from the fit were used to calculate the change in trapped aqueous volume in response to the perturbation. The average calculated lower-layer volume was 93 ± 1% of the original volume, corresponding to $[Na^+_{(lower)}]$ ≈0.54 M, assuming that no ions leaked across the BLM. The value obtained for $[Na+_{(lower)}]$ suggests that, when $[Na^+_{(outer)}]$ is adjusted from 0.50 M to 0.53 M, the system responds to osmotic stress by reducing the trapped aqueous volume to adjust $[Na^+_{(lower)}]$ to a similar value.

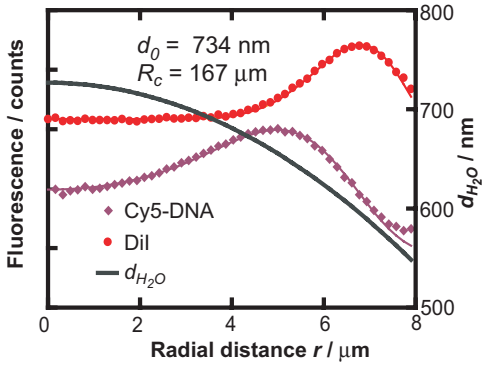

Fig. 4. Fluorescence intensity data for DiI and Cy5-DNA for the same well as in Fig. 3. Best-fit analysis by 2C-FLIC is marked as solid lines. The bilayer shape corresponding to this fit is marked in black, with the fit parameters, d_0 and R_c, shown. These agree closely with the values from the VIA-FLIC analysis in Fig. 3.

Discussion

Our system differs from those described in the classic BLM literature because our goal is subdiffraction optical imaging by FLIC, i.e., we require a bilayer membrane with large (>10 μm) lateral dimensions and with a mirrored surface <1 μm from the intended site of membrane formation. These requirements led us to incorporate a passivated yet hydrophilic well, with different chemical functionality to the hydrophobic aperture, to maintain the required water reservoir. The reservoir is small (subpicoliter) and was disrupted by typical BLM formation approaches, such as direct addition of lipid dissolved in organic solvent (32, 33) or spreading from an air/water interface (29, 34). For the trapped aqueous reservoir to consistently survive, addition of PEG (1.5%) to the trapped aqueous solution and a more gentle lipid addition as small vesicles in the upper aqueous layer were required.

Although the images presented here show only a few bilayer-covered wells, many more were usually present, although these wells themselves were a small fraction of all of the wells on the substrate; most wells were either open or covered by a thicker decane film. However, true bilayers could be distinguished visually and by using simple tests (*SI Text*) and could be shown to support simple functional membrane proteins such as gramicidin.

VIA-FLIC and 2C-FLIC, although both based on interferometry, are distinct methods for determining the bilayers' geometric parameters. There is substantial agreement between the methods for the 10 wells in Fig. 5, and the methods can readily distinguish bilayers of different curvature. Also, the geometric parameters obtained through interferometry are consistent with

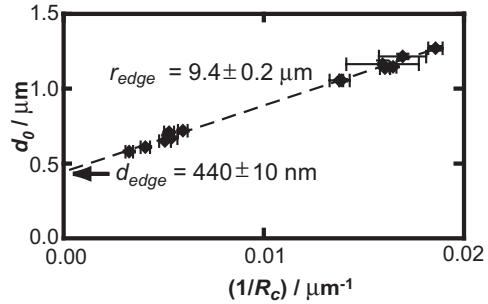

Fig. 5. d_0 values plotted against 1/R_c values determined by VIA-FLIC on 14 wells analyzed as spherical caps, giving the edge location (r_{edge}, d_{edge}) (see Eq. 2 and Fig. S6). Errors shown are the percent difference between VIA-FLIC and 2C-FLIC fit results for 10 wells and half the maximum percent difference for 4 wells whose bilayer positions were not determined by 2C-FLIC.

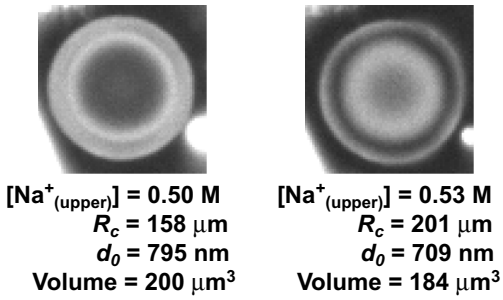

Fig. 6. Changing [Na$^+$$_{(upper)}$] affects bilayer position. Shown are Cy5-DNA fluorescence images of a well at [Na$^+$$_{(upper)}$] = 0.50 M and 0.53 M, with calculated trapped aqueous volumes (calculated by 2C-FLIC) marked.

known parameters of the system such as well depth and width. However, the results suggest that neither method is currently able to measure absolute position with subnanometer accuracy. One intrinsic limitation is the lateral resolution limit imposed by optical diffraction, given by the Abbé equation. Under our imaging conditions, this limit is approximately half the wavelength of light, or ≈300 nm. For a spherical cap-shaped bilayer with R_c = 100 μm, this lateral range corresponds to a vertical position range of 3 nm near the center of the well (r = 1 μm), increasing to 24 nm at r = 8 μm. Thus, lateral blurring, not included in our fitting model, may affect data acquired near the well edges, especially for more highly curved bilayers. Also, the models' dipole orientation parameters assume a flat planar geometry, even though the bilayer is curved. Other errors caused by background or photomask alignment (for VIA-FLIC) may also limit accuracy.

The observed bilayer curvature is an interesting result. Because the curvature is very slight (R_c ≈100 μm) and the interfacial tension of freestanding lipid bilayers is predicted to be very small (< ≈5 mN/m) (35, 36), the pressure difference supporting the spherical curvature, determined from the Young-Laplace equation, should be very small (≈50 Pa). This pressure difference corresponds to a small difference in osmotic pressure of <0.1 mM. If osmotic pressure alone determines curvature, one would expect that changes in the osmolarity of the upper aqueous layer would have drastic effects on bilayer curvature. Indeed, the bilayer curvature does change but less than would be expected in this scenario (Fig. 6).

The results instead suggest that the effect of an osmotic perturbation is water permeation, analogous to the effect in giant vesicles subjected to osmotic stress (37). In this model, when the decane droplet, in contact with the hydrophobic gold surface, is spread between 2 water layers, it is pinned at the well edges at a contact angle determined by the interface energies between decane, water, and the gold monolayer, leading to a stable 3-layer system. Upon adding lipid vesicles, the decane/water interface energy is reduced, reducing the contact angle of decane on the hydrophobic gold, and the decane thins to a lipid bilayer that is substantially water-permeable (38) (see *SI Text*). The trapped aqueous layer, containing 1.5% PEG, initially has higher osmolarity than the bulk, and water flow establishes an equilibrium bilayer curvature and osmotic pressure difference that would also satisfy the asymmetric boundary conditions imposed by the BLM annulus in contact with the edge of the well (39). More extensive investigation of osmotic effects show more complicated, history-dependent behavior that merits further exploration. A range of experimental variations or improvements could also be considered. Alternative assembly approaches, such as giant vesicle rupture over wells, could replace the decane film approach and give quite different behavior. Also,

a design incorporating substrate electrodes would greatly expand possible applications.

Materials and Methods

Substrate Preparation (Fig. S1). Substrates were fabricated by using standard lift-off processing. SiO_2 of thickness ≈400 nm was formed by thermal oxidation on a Si wafer. Patterns for circular wells with diameter 5, 10, and 20 μm (thousands per 8 × 8 mm chip) were defined by using photoresist (Fig. S1*A*). Thin films of titanium (5 nm), Au (50 nm), and Cr (50 nm) were deposited by evaporation (Fig. S1*B*), and the resist was removed in acetone (Fig. S1*C*). The circular regions of exposed SiO_2 were etched anisotropically by using a CHF_3/O_2 reactive ion etch to make shallow wells in the wafer (Fig. S1*D*). The etch was timed to stop with a thin layer of oxide (≈10–30 nm) remaining, leaving the Si/SiO_2 interface undisturbed so the Si mirror was preserved. The upper Cr layer was removed by extended soaking in Cr etchant (CR-14, Cyantek) (Fig. S1*E*), giving a final well depth of ≈450 nm. The wafers were diced into 8-mm square chips for bilayer preparation.

For chemical functionalization (Fig. S1*F*), substrates were treated in a plasma cleaner under air, then immersed in a 1 mM solution of octadecanethiol (Sigma) in ethanol with gentle warming for 12–18 h. They were then rinsed extensively in ethanol and dried under nitrogen and by heating on a hotplate at ≈110 °C. The substrates were then immersed in a 1 mM solution of 2-[methoxy(polyethyleneoxy)propyl]trimethoxysilane (Gelest) in dry toluene for 4–5 h. The substrates were cleaned by sonication in fresh toluene, followed by extensive rinsing with ethanol and drying under nitrogen. Substrates were used within 2 d of surface functionalization.

Bilayer Formation (Fig. S2). A DNA 24-mer labeled with Cy5 at the 3′ end was synthesized on a DNA synthesizer and coupled to a lipid molecule at the 5′ end to make Cy5-DNA, as described in ref. 28. Small, unilamellar vesicles consisting of 49.5 mol% palmitoyloleoylphosphatidylcholine (POPC) (Avanti Polar Lipids), 49.5 mol% diphytanoylphosphatidylcholine (DPhPC) (Avanti), and DiI (Molecular Probes) were prepared by rehydration of dried lipid stocks and extrusion through a 0.1-μm polycarbonate filter (Whatman) at a nominal concentration of 5 mg/mL of lipid. Buffers used for vesicle and sample preparation contained 0.50 M NaCl and were at either pH ≈7 (10 mM MOPS) or pH ≈6 (10 mM MES). At least 4 h before use, Cy5-DNA was dissolved in 1:1 water/acetonitrile and vesicles were added to the mixture, for a final concentration of 200 DNA/vesicle, or ≈0.2 mol% DNA.

Experiments on the chips were performed in a shallow, polydimethylsiloxane chamber. The chamber was filled with buffer with 1.5% wt/wt PEG (typical molecular weight 2000, Sigma) and 10 μM CF (Sigma) added. Decane (20 μl) was applied to the chip from a pipette, and the solution in the chamber was washed extensively (Fig. S2*A*) with buffer that did not contain PEG or CF. Vesicles (≈400 μg) of the desired lipid composition were added to the bulk solution (Fig. S2*B*), and the substrate was left covered for at least 8 h. After further washing, fluorescence microscopy images of the sample were examined. If the decane layer had not spontaneously thinned (Fig. S2 *C* and *D* and Fig. S3) to form freestanding bilayers on at least some part of the sample, a small air bubble (1.1 μl from a Pipetman tip) was delicately brushed across the surface to thin the decane layer. This process was repeated until freestanding bilayers (Fig. S2*D*) were observed. Tests for bilayer formation, such as heavy-atom quenching and FRAP, were performed (Fig. S4).

Fluorescence Imaging. Fluorescence microscopy was performed on a Nikon E800 epifluorescence microscope using a 40×, N.A. 0.8 water dipping objective with a mercury arc lamp (103D, Ushio) that had been passed through a light scrambler (Technical Video) as a light source. Samples were imaged by using Texas Red (HQ560/55x, Q595LP, HQ645/75m), EGFP (HQ470/40x, Q495LP, HQ525/50m), and Cy5 (HQ620/60x, Q660LP, HQ700/75m) filter sets (Chroma Technology). For VIA-FLIC experiments, samples were imaged through a series of annular photomasks of variable radii corresponding to different angles of incidence, θ_{inc}, each annulus having a width of 250 μm mounted on a motorized stage (26). Images were collected and initially processed in MetaMorph (Molecular Devices).

Gramicidin Insertion (Fig. 2 and Fig. S5). Vesicles were prepared as described above except that the lipid stock (in chloroform) was mixed with 0.01 mol% gramicidin D (Sigma) before being dried and rehydrated. Bilayers were prepared from these vesicles with ≈10 μM trapped CF. Exchanging different buffers into the bulk (upper) aqueous layer produced changes in CF fluorescence intensity that were monitored by microscopy.

FLIC and VIA-FLIC Analysis. Well centers were determined empirically in Matlab by finding the center position that minimized the SE of the radial fluorescence intensity. Radial fluorescence intensities were binned in 0.5 pixel increments. Because the CCD pixel size was 6.45 × 6.45 μm^2 and images were binned 2 × 2, this increment corresponds to a distance of 161.25 nm.

VIA-FLIC data were fit in Matlab. The best fits were obtained by using the described model (26) with the addition of a variable background term. The background term took the form $b_1 + \sin(\theta_{inc})\, b_2$, with θ_{inc} defined as the excitation angle of incidence, and b_1 and b_2 variables that were constrained to be constant for data from a given well. For excitation by a uniform circular disk, the excitation intensity is proportional to the annular area, itself proportional to the annular radius, which is proportional to $\sin(\theta_{inc})$ (26). Thus, the background term includes terms proportional to and independent of the excitation intensity. Because of the inclusion of the background term, the relative values of fluorescence-emission intensity at different distances from the mirror could not be ignored (26); rather, an emission intensity term was also included by integration over the N.A. of the objective (22). Initially, each radial distance in the well was fit with a discrete d_{H_2O} value (the discrete model). An additional scaling factor a was also required. Thus, each intensity data point was fit to the equation:

$$I_{exp}(r,\ \theta_{inc}, d_{H_2O}) = a \cdot I_{calc}(r,\ \theta_{inc}, d_{H_2O}) + b_1 + b_2 \cdot \sin\theta_{inc}. \quad [3]$$

The fixed parameters of the system were as described in refs. 22 and 26. Briefly, the thickness of the bilayer hydrophobic region was set at 3.78 nm. DiI was modeled as equally distributed in 2 layers 0.9 Å from the top and bottom bilayer interfaces. Transition dipole orientations were fixed at 62° relative to bilayer normal (22). Transmission data for the microscope filters and absorption and emission spectra for the dyes were provided by the manufacturers and used as wavelength-dependent functions in the integration of the model over wavelength (22).

The initial analysis of the interference rings gave VIA-FLIC fits to data that approximated a spherical cap. To extract useful geometric parameters, bilayer data were fit as a spherical cap (the spherical cap model). In this approach, a bilayer cross-section was treated as an arc of a circle, center (0, d_0–R_c), radius R_c, for d_0 and R_c the trapped water layer thickness at the center of the well and the radius of curvature, respectively (Fig. S6). Thus, d_{H_2O} was a function of r, d_0, and R_c. Rather than fitting Eq. **3** separately for each r, a system of equations was optimized simultaneously for the best possible values of d_0, R_c, a, b_1, and b_2.

2C-FLIC data for DiI and Cy5 were fit in Matlab with a spherical cap model similar to the VIA-FLIC model. Integration of excitation illumination was performed over the objective N.A. (22, 25). The refined parameters were d_0 and R_c, and background and scaling factors for each dye, b_{DiI}, b_{Cy5}, a_{DiI}, a_{Cy5}, giving the equation:

$$I_{exp,x} = a_x \cdot I_{calc}(R_c, d_0) + b_x. \quad [4]$$

In Eq. **4**, x is either DiI or Cy5, and I is a vector of intensities (over r). The equations for the 2 dyes were optimized simultaneously. Note that the background for 2C-FLIC is scalar because annular photomasks were not used in this experiment. In addition to the parameters used for VIA-FLIC, Cy5 was modeled at a distance of 6 nm above the upper bilayer/water interface. The absorption and emission dipoles were usually defined as freely rotating; however, marginally better fits of the Cy5 data were obtained with absorption and emission transition dipole orientations of 62°. This result may indicate partial insertion of Cy5 into the bilayer, or it may be correcting for other systematic simplifications in the model.

Effect of Salt. To measure the effect of changing $[Na^+_{(upper)}]$, a BLM sample was prepared in 0.50 M NaCl (bulk solution volume ≈1.2 mL), and 6 wells with BLMs were imaged. To increase $[Na^+_{(upper)}]$ to 0.53 M, 1 M NaCl (75 μl) was added to the sample. Fluorescence images for 2C-FLIC analysis were acquired before and after aliquot addition.

ACKNOWLEDGMENTS. We thank Profs. Nick Melosh, Merritt Maduke, and Stephen White for useful insights and suggestions. The Cy5-DNA-lipid conjugate was synthesized by Mark Chan and Bettina van Lengerich (Stanford University, CA). This work was supported by National Institutes of Health Grant GM069630, the National Science Foundation Biophysics Program, Stanford Bio-X Interdisciplinary Initiatives Program, and Benchmark Stanford Graduate fellowship and Center for Probing the Nanoscale Graduate Prize fellowship (to P.V.G.).

1. Tien HT, Ottova-Leitmannova A (2003) *Planar Lipid Bilayers (BLMs) and Their Applications* (Elsevier, Boston).
2. Rentschler M, Fromherz P (1998) Membrane-transistor cable. *Langmuir* 14:547–551.
3. Hennesthal C, Drexler J, Steinem C (2002) Membrane-suspended nanocompartments based on ordered pores in alumina. *ChemPhysChem* 3:885–889.
4. Funakoshi K, Suzuki H, Takeuchi S (2006) Lipid bilayer formation by contacting monolayers in a microfluidic device for membrane protein analysis. *Anal Chem* 78:8169–8174.
5. Malmstadt N, Nash MA, Purnell RF, Schmidt JJ (2006) Automated formation of lipid-bilayer membranes in a microfluidic device. *Nano Lett* 6:1961–1965.
6. Sandison ME, Zagnoni M, Morgan H (2007) Air-exposure technique for the formation of artificial lipid bilayers in microsystems. *Langmuir* 23:8277–8284.
7. Suzuki H, Tabata KV, Noji H, Takeuchi S (2006) Highly reproducible method of planar lipid bilayer reconstitution in polymethyl methacrylate microfluidic chip. *Langmuir* 22:1937–1942.
8. Kang X-F, Cheley S, Rice-Ficht AC, Bayley H (2007) A storable encapsulated bilayer chip containing a single protein nanopore. *J Am Chem Soc* 129:4701–4705.
9. Jeon TJ, Malmstadt N, Schmidt JJ (2006) Hydrogel-encapsulated lipid membranes. *J Am Chem Soc* 128:42–43.
10. Weiskopf D, Schmitt EK, Kluhr MH, Dertinger SK, Steinem C (2007) Micro-BLMs on highly ordered porous silicon substrates: Rupture process and lateral mobility. *Langmuir* 23:9134–9139.
11. Borisenko V, et al. (2003) Simultaneous optical and electrical recording of single gramicidin channels. *Biophys J* 84:612–622.
12. Ide T, Takeuchi Y, Aoki T, Yanagida T (2002) Simultaneous optical and electrical recording of a single ion-channel. *Jpn J Physiol* 52:429–434.
13. Ries RS, Choi H, Blunck R, Bezanilla F, Heath JR (2004) Black lipid membranes: Visualizing the structure, dynamics, and substrate dependence of membranes. *J Phys Chem B* 108:16040–16049.
14. Thompson JR, Heron AJ, Santoso Y, Wallace MI (2007) Enhanced stability and fluidity in droplet on hydrogel bilayers for measuring membrane protein diffusion. *Nano Lett* 7:3875–3878.
15. Sackmann E (1996) Supported membranes: Scientific and practical applications. *Science* 271:43–48.
16. Chan Y-HM, Boxer SG (2007) Model membrane systems and their applications. *Curr Opin Chem Biol* 11:581–587.
17. Knoll W, Köper I, Naumann R, Sinner E-K (2008) Tethered bimolecular lipid membranes-A novel model membrane platform. *Electrochim Acta* 53:6680–6689.
18. Tanaka M, Sackmann E (2005) Polymer-supported membranes as models of the cell surface. *Nature* 437:656–663.
19. Wong AP, Groves JT (2002) Fluorescence interference and energy transfer imaging of nanometer-scale topography at an intermembrane junction. *Biophys J* 82:160A.
20. Parthasarathy R, Groves JT (2004) Protein patterns at lipid bilayer junctions. *Proc Natl Acad Sci USA* 101:12798–12803.
21. Kaizuka Y, Groves JT (2006) Hydrodynamic damping of membrane thermal fluctuations near surfaces imaged by fluorescence interference microscopy. *Phys Rev Lett* 96:118101–118104.
22. Lambacher A, Fromherz P (2002) Luminescence of dye molecules on oxidized silicon and fluorescence interference contrast microscopy of biomembranes. *J Opt Soc Am B* 19:1435–1453.
23. Lambacher A, Fromherz P (1996) Fluorescence interference-contrast microscopy on oxidized silicon using a monomolecular dye layer. *Appl Phys A: Mater Sci Process* 63:207–216.
24. Kiessling V, Tamm LK (2003) Measuring distances in supported bilayers by fluorescence interference-contrast microscopy: Polymer supports and SNARE proteins. *Biophys J* 84:408–418.
25. Ajo-Franklin CM, Yoshina-Ishii C, Boxer SG (2005) Probing the structure of supported membranes and tethered oligonucleotides by fluorescence interference contrast microscopy. *Langmuir* 21:4976–4983.
26. Ajo-Franklin CM, Ganesan PV, Boxer SG (2005) Variable incidence angle fluorescence interference contrast microscopy for Z-imaging single objects. *Biophys J* 89:2759–2769.
27. Kalyankar ND, et al. (2006) Arraying of intact liposomes into chemically functionalized microwells. *Langmuir* 22:5403–5411.
28. Chan Y-HM, van Lengerich B, Boxer SG (2008) Lipid-anchored DNA mediates vesicle fusion as observed by lipid and content mixing. *Biointerphases* 3:FA17–FA21.
29. Montal M, Mueller P (1972) Formation of bimolecular membranes from lipid monolayers and a study of their electrical properties. *Proc Natl Acad Sci USA* 69:3561–3566.
30. Hladky SB, Haydon DA (1972) Ion transfer across lipid membranes in the presence of gramicidin A: I. Studies of unit conductance channel. *Biochim Biophys Acta* 274:294–312.
31. Urry DW (1971) The gramicidin A transmembrane channel: A proposed (L,D) helix. *Proc Natl Acad Sci USA* 68:672–676.
32. White SH (1978) Formation of solvent-free black lipid bilayer membranes from glyceryl monooleate dispersed in squalene. *Biophys J* 23:337–348.
33. Mueller P, Wescott WC, Rudin DO, Tien HT (1963) Methods for formation of single bimolecular lipid membranes in aqueous solution. *J Phys Chem* 67:534–535.
34. Mayer M, Kriebel JK, Tosteson MT, Whitesides GM (2003) Microfabricated teflon membranes for low-noise recordings of ion channels in planar lipid bilayers. *Biophys J* 85:2684–2695.
35. Feller SE, Pastor RW (1996) On simulating lipid bilayers with an applied surface tension: Periodic boundary conditions and undulations. *Biophys J* 71:1350–1355.
36. Jahnig F (1996) What is the surface tension of a lipid bilayer membrane? *Biophys J* 71:1348–1349.
37. Olbrich K, Rawicz W, Needham D, Evans E (2000) Water permeability and mechanical strength of polyunsaturated lipid bilayers. *Biophys J* 79:321–327.
38. Israelachvili JN (1992) *Intermolecular and Surface Forces* (Academic, London).
39. White SH, Petersen DC, Simon S, Yafuso M (1976) Formation of planar bilayer membranes from lipid monolayers. A critique. *Biophys J* 16:481–489.